Vol. 5(14) Jan.2015, PP. 000-000

Contents list available at IJMEC

International Journal of Mechatronics, Electrical and Computer Technology (IJMEC)

Journal Homepage: www.aeuso.org

ISSN: 2305-0543

Research and Development of Cascade Induction Mode Performance Analysis in Brushless Doubly-Fed Induction Machine

Alireza Nasiri[1]*, Omid Mehdiyar[1], Hamed Gorginpur[2], Mahdi Taghizadeh[1]

[1] Department of Electrical Engineering, Kazeroon branch, Islamic Azad University, Fars, Iran

[2] Khalij Fars University Of Bushher, Bushher, Iran

+98 917 689 4009

***Corresponding Author's E-mail** ar.na30ri.68@gmail.com*

Abstract

This paper presents fundamental aspects of the cascade induction mode of brushless doubly fed Induction Machine. The investigation is performed by analyzing the spatial harmonic contents of the rotor magnetic flux density. The direct cross couplings between stator and rotor fields as well as, indirect cross coupling between stator fields by the special rotor of this machine is described. Furthermore, loss analysis of the machine in various modes is presented and the torque- speed curves for asynchronous modes are obtained. A 2-D magneto-dynamic finite element model based on the D-180 4/8 pole prototype machine is extracted and simulated to verify the results.

Keywords: *Brushless doubly fed machine (BDFM), nested loop rotor, cascade induction mode, direct and indirect cross coupling, spatial harmonic.*

1. Introduction

The conceptual idea of the machines with two stator windings can be traced to some publications in the 1900s [1-3]. From the stator winding point of view, dual-stator winding machines have been categorized as *split-wound* and *self-cascaded* [4]. The split-wound dual-winding machine was proposed to improve the power capability of large synchronous generators and to achieve better drive reliability resulting from its inherent redundancy [5]. The second type, the self-cascaded machine or the brushless doubly-fed machine (BDFM), with two sets of stator windings, which do not couple directly but via the intermediate action of a special rotor, was introduced by Hunt in 1907 [2]. The special rotor structure increases the manufacturing cost and the complexity of the machine and produces undesirable spatial harmonics which decrease machine efficiency. But the brushless doubly fed machine shows commercial advantages because of the fractionally rated converter, and absence of the brush gear. The major application of BDFM is in wind generation, especially in harsh conditions, where it requires lower maintenance. Furthermore, it can be used as an adjustable speed drive [6, 7].

Article History:

IJMEC DOI: xxxx

Received Date: xxxx

The BDFM has two balanced three-phase windings on its stator. One of them is the power winding with P_p pole pairs, which is directly connected to the grid, and the control winding with P_c pole pairs, which is connected to the grid via a bidirectional fractional rated frequency converter (Figure 1). There are some rules on the selection of the stator windings pole number to avoid electromagnetic coupling between them [8].

The rotor should couple the power and control windings magnetic fields, in the appropriate manner. There are some suggestions about the rotor configuration [9]. The most popular structure is nested loop rotor, which was proposed by Broadway and Burbridge [10] (Figure 2). In this structure, the rotor consists of a number of nests and some loops in each nest which are short circuited through an end ring. The number of nests should be equal to the summation of the number of power winding and control winding pole pairs to provide indirect cross coupling between the fields of the stator windings ($P_r=P_p+P_c$).

The modeling and performance analysis of the BDFM has been examined in many publications. However, there is no comprehensive discussion on the electromagnetic phenomena that takes place and results in the three modes of operation. An alternative formulation of BDFM operation in synchronous mode has been published recently [11]. The paper presents a precise characterization of all magnetic field components, which can be used in the machine design process and investigate the appropriate rotor configuration.

This paper presents the characteristics of the BDFM in simple induction, cascade induction and synchronous modes of operation and also, describes the direct and indirect cross coupling by simple electromagnetic relations. To simplify the analysis procedure and extraction of the relations, it is supposed that the nested loop rotor has one loop in each nest. As in the case of squirrel cage induction machine, increasing the number of rotor bars decreases the spatial harmonic contents of the rotor flux and its leakage inductance, and therefore, results in better performance characteristics. A 2-D magnetodynamic finite element model of the D-180 frame prototype BDFM is used for verification.

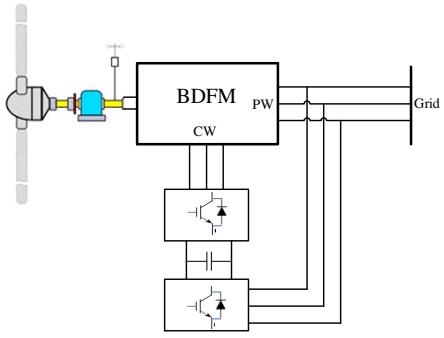

Figure 1. A wind turbine configuration based on BDFM.

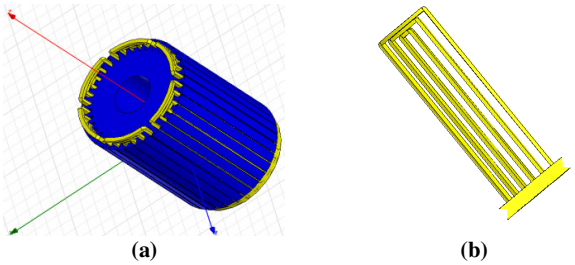

Figure 2. (a) Nested loop rotor with six nests and three loops per

2- General Investigations

2-1 Magnetic Fields

The magnetic field density of the power winding (B_p) in its reference and in the rotor reference frames are stated in Equations (1) and (2), respectively.

$$B_p(t,\theta_p) = B_{p,\max}\cos\left(\omega_p t - P_p\theta_p\right) \quad (1)$$

$$B_p(t,\theta_r) = B_{p,\max}\cos\left(\left(\omega_p - P_p\omega_r\right)t - P_p\theta_r\right) \quad (2)$$

Where ϑ_p and ϑ_r are the mechanical angle around the air gap in power winding and rotor reference frames, respectively. ω_p and ω_r represent the angular frequencies of the power winding supply and rotor, respectively.

The rotating magnetic field induces an emf in the rotor bars according to $e = \vec{v}\times\vec{B}.\vec{l}$, which has the following distribution in the rotor reference frame,

$$e_{rp}(t,\theta_r) = lr\frac{\omega_p - P_p\omega_r}{P_p}B_{p,\max}\cos\left(\left(\omega_p - P_p\omega_r\right)t - P_p\theta_r\right) \quad (3)$$

where*l* and *r* are the machine axial length and the air gap radius, respectively.

As stated, the number of rotor nests equals to P_p+P_c. The arrangement of the rotor with one loop per nest and the nest span of $2\pi(1/P_r - 1/N_{rb})$ are depicted in Figure 3 where N_{rb} represents the number of rotor slots.

The emf induced in one loop can be calculated by subtracting two induced bar emfs as Equation (4).

$$\Delta V_{rp}^{k}(t,\theta_r) = lr\frac{\omega_p - P_p\omega_r}{P_p}B_{p,\max}\times\left[\cos\left(\left(\omega_p - P_p\omega_r\right)t - P_p\left(\theta_{r0} + \frac{2k\pi}{P_r} + \frac{\pi}{N_{rb}}\right)\right) - \cos\left(\left(\omega_p - P_p\omega_r\right)t - P_p\left(\theta_{r0} + \frac{2(k+1)\pi}{P_r} + \frac{\pi}{N_{rb}}\right)\right)\right] \quad (4)$$

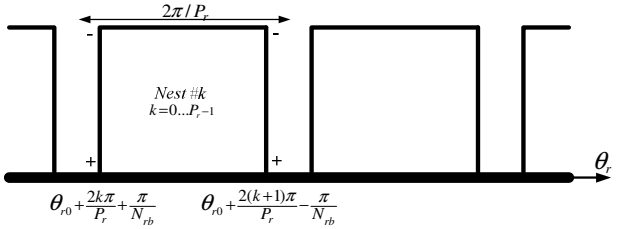

Figure 3. Nested loop rotor with one loop per nest.

With somesimplifications, $\Delta V_{rp}^{k}(t,\theta_r)$ can be expressed as,

$$\Delta V_{rp}^{k}(t,\theta_k) = 2lr\frac{\omega_p - P_p\omega_r}{P_p}B_{p,\max}\times\sin\left(\pi P_p\left(\frac{1}{P_r} - \frac{1}{N_{rb}}\right)\right)\sin\left(\left(\omega_p - P_p\omega_r\right)t - P_p\theta_k\right) \quad (5)$$

where

$$\theta_k = \theta_{r0} + \frac{2\pi}{P_r}\left(k + \frac{1}{2}\right) \quad (6)$$

This voltage produces a loop current through the loop impedance,

$$i_{rp}^{k}(t,\theta_k) = 2lr\frac{\omega_p - P_p\omega_r}{P_p\sqrt{R_l^2 + \left(\omega_p - P_p\omega_r\right)^2 L_l^2}}B_{p,\max}\times\sin\left(\pi P_p\left(\frac{1}{P_r} - \frac{1}{N_{rb}}\right)\right)\times\sin\left(\left(\omega_p - P_p\omega_r\right)t - P_p\theta_k - \tan^{-1}\frac{\left(\omega_p - P_p\omega_r\right)L_l}{R_l}\right) \quad (7)$$

whereR_l and L_l are the resistance and leakage inductance of the loop, respectively. The maximum

value of the loop current depends only on the rotor angular velocity, that is:

$$I_{rp,\max}(\omega_r) = 2lr\frac{\omega_p - P_p\omega_r}{P_p\sqrt{R_l^2+(\omega_p-P_p\omega_r)^2L_l^2}}B_{p,\max}\sin\left(\pi P_p\left(\frac{1}{P_r}-\frac{1}{N_{rb}}\right)\right) \quad (8)$$

so

$$i_{rp}^k(t,\theta_k) = I_{rp,\max}^k(\omega_r)\sin\left(\left(\omega_p - P_p\omega_r\right)t - P_p\theta_k - \varphi_{nest}(\omega_r)\right) \quad (9)$$

where

$$\varphi_{nest}(\omega_r) = \tan^{-1}\frac{(\omega_p - P_p\omega_r)L_l}{R_l} \quad (10)$$

The rotor currents produce magnetic motive force in the air gap, which can be calculated by the production of the current and turn function of rotor. The distribution of the k^{th} nest MMF as a function of the rotor angular position in the rotor reference frame is shown in Figure 4.

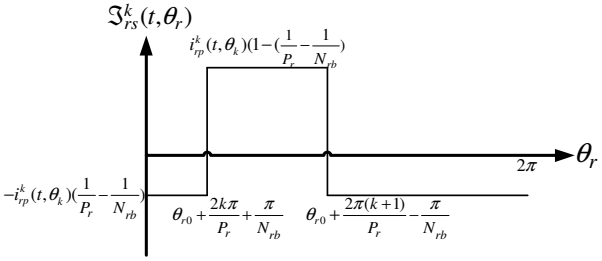

Figure 4. Spatial distribution of the k[th] nest ampere turn.

Fourier series representation of this spatial MMF function has the following coefficients,

$$a_n^k = \frac{2i_{rp}^k(t,\theta_k)}{n\pi}\sin\left(n\pi\left(\frac{1}{P_r}-\frac{1}{N_{rb}}\right)\right)\cos(n\theta_k) \quad (11)$$

$$b_n^k = \frac{2i_{rp}^k(t,\theta_k)}{n\pi}\sin\left(n\pi\left(\frac{1}{P_r}-\frac{1}{N_{rb}}\right)\right)\sin(n\theta_k) \quad (12)$$

Fourier series of the rotor MMF can be obtained by the summation of MMF Fourier series of all nests as (13).

$$\Im_{rp}(t,\theta_r) = \sum_{n=1}^{\infty}\sum_{k=0}^{P_r-1}\frac{2I_{rp,\max}^k(\omega_r)}{n\pi}\sin\left(n\pi\left(\frac{1}{P_r}-\frac{1}{N_{rb}}\right)\right)\times\sin\left(\left(\omega_p-P_p\omega_r\right)t-P_p\theta_k-\varphi_{nest}(\omega_r)\right)\cos\left(n\left(\theta_r-\theta_k\right)\right) \quad (13)$$

Since $\theta_k = \frac{2\pi}{P_r}(k+1/2)$, $\sum_{k=0}^{P_r-1}$ is equivalent to the integration over θ_k in [0, 2π] interval.

The production of the two terms containing ϑ_k in Equation (13) can be written in summation form as,

$$\sin\left(\left(\omega_p-P_p\omega_r\right)t-P_p\theta_k-\varphi_{nest}(\omega_r)\right)\cos\left(n\left(\theta_r-\theta_k\right)\right) = \frac{1}{2}\Big[\sin\left(\left(\omega_p-P_p\omega_r\right)t-\left(P_p+n\right)\theta_k+n\theta_r-\varphi_{nest}(\omega_r)\right)+ \sin\left(\left(\omega_p-P_p\omega_r\right)t-\left(n-P_p\right)\theta_k-n\theta_r-\varphi_{nest}(\omega_r)\right)\Big] \quad (14)$$

Substituting $n=P_c+hP_r$, h=0,1,2,…, in the first term of the right hand side of (14), the coefficient of k will be $-2\pi(h+1)$, which eliminates the dependency on the k factor, and therefore, the result of the summation will be non zero. Similarly, if $n=P_p+hP_r$, h=0,1,2,…, in the second term of the right hand, the coefficient of k will be $2\pi h$, which also leads to non zero value for the summation. Hence, space harmonic orders $n=P_p+hP_r$ and $n=P_c+hP_r$ appear in the rotor produced MMF in the air gap due to power winding rotating field. All harmonics have the same time frequency. However, the rotation direction of $n=P_p+hP_r$ and $n=P_c+hP_r$ orders are in the same and the opposite direction, respectively, in

comparison with the power winding flux.
Similarly, it can be shown that if the power winding is opened and in turn, the control winding is supplied, the rotor will produce an MMF with spatial harmonic orders $n=P_p+hP_r$ and $n=P_c+hP_r$, which rotate in the opposite and same direction with respect to the control winding flux, respectively.

2.2. Direct and Indirect Cross Coupling

Among the rotor field space harmonics due to the field of the power (/control) winding, the P_p (/P_c) pole pair harmonic field couples with the power (/control) winding field. This mechanism is called "direct cross coupling". Similarly, the rotor field harmonic which has P_c (/P_p) pole pairs due to the field of the power (/control) winding, can couple with the control (/power) winding, if they have also same time frequency. However, this mechanism is called "indirect cross coupling".

The rotor MMF harmonics with P_p and P_c pole pairs corresponding to the power winding magnetic field are presented in Equations (15) and (16), respectively.

$$\Im_{rp,P_p}(t,\theta_r)=\frac{2lrP_rB_{p,\max}\sin^2\left(\pi P_p\left(\frac{1}{P_r}-\frac{1}{N_{rb}}\right)\right)}{\pi P_p^2\sqrt{R_l^2+\left(\omega_p-P_p\omega_r\right)^2L_l^2}}\times\sin\left[\left(\omega_p-P_p\omega_r\right)t-P_p\theta_r-\varphi_{nest}(\omega_r)\right] \quad (15)$$

$$\Im_{rp,P_c}(t,\theta_r)=\frac{-2lrP_rB_{p,\max}\sin\left(\pi P_p\left(\frac{1}{P_r}-\frac{1}{N_{rb}}\right)\right)\sin\left(\pi P_c\left(\frac{1}{P_r}-\frac{1}{N_{rb}}\right)\right)}{\pi P_pP_c\sqrt{R_l^2+\left(\omega_p-P_p\omega_r\right)^2L_l^2}}\times\sin\left[\left(\omega_p-P_p\omega_r\right)t-P_c\theta_r-\varphi_{nest}(\omega_r)\right] \quad (16)$$

The amplitudes of these components are related just to the shaft rotational speed. Considering Equation (17), where g is the air gap width, the produced magnetic field densities can be written as Equations (18) and (19).

$$\Im=\frac{\mu_0}{g}B \quad (17)$$

$$B_{rp,P_p}(t,\theta_r)=B_{rp,P_p,\max}(\omega_r)\sin\left[\left(\omega_p-P_p\omega_r\right)t-P_p\theta_r-\varphi_{nest}(\omega_r)\right] \quad (18)$$

$$B_{rp,P_c}(t,\theta_r)=B_{rp,P_c,\max}(\omega_r)\sin\left[\left(\omega_p-P_p\omega_r\right)t-P_c\theta_r-\varphi_{nest}(\omega_r)\right] \quad (19)$$

The mechanical angular frequency of $B_{rp,Pc}(t,\theta_r)$ equals $(\omega_p-P_p\omega_r)/P_c$ in the opposite direction with respect to the rotor. Hence, the field mechanical angular frequency from the control winding's point of view is,

$$\omega_r-\frac{\omega_p-P_p\omega_r}{P_c}=\frac{P_r\omega_r-\omega_p}{P_c} \quad (20)$$

Therefore,

$$B_{rp,P_c}(t,\theta_c)=B_{rp,P_c,\max}(\omega_r)\sin\left[\left(\omega_p-P_r\omega_r\right)t+P_c\theta_c-\varphi_{nest}(\omega_r)\right] \quad (21)$$

2.3. Induced EMF in Control Winding

To find the induced voltage in each phase of the control winding due to $B_{rp,P_c}(t,\theta_c)$, first the induced emf in one coil with N_c series turn positioned at θ_c angle should be calculated.

$$e_c^{rp,P_c}(t,\theta_c)=N_clr\frac{\omega_p-P_r\omega_r}{P_c}B_{rp,P_c,\max}(\omega_r)\times\sin\left[\left(\omega_p-P_r\omega_r\right)t+P_c\theta_c-\varphi_{nest}(\omega_r)\right] \quad (22)$$

Considering N_s as the number of stator slots, the distance between two consecutive slots is $2\pi/N_s$, and the number of slots in each pole and phase is $N_s/6P_c$. Considering one layer full pitch winding, the induced voltage in each phase of the control winding can be represented as Equation (23).

$$V_c^{rp,P_c}(t)=2P_c\sum_{k=0}^{\frac{N_s}{6P_c}-1}N_c lr\frac{\omega_p-P_r\omega_r}{P_c}B_{rp,P_c,\max}(\omega_r)\times\sin\left[\left(\omega_p-P_r\omega_r\right)t+P_c\left(\theta_{c0}+k\frac{2\pi}{N_s}\right)-\varphi_{nest}(\omega_r)\right] \quad (23)$$

It is evident from Equation (23) that the amplitude and frequency of the induced voltage are zero at the natural speed ($\omega_r=\omega_n=\omega_p/p_r$). If the voltage can produce a current, the air gap flux produced by the currents for $\omega_r<\omega_n$ and $\omega_r>\omega_n$ will rotate in the opposite and the same direction with respect to the rotor, respectively.

3. Cascade Induction Mode

This mode of operation occurs when one of the stator windings are supplied, while another is short circuited. In fact, BDFM in the cascade mode can be considered as two induction machines with rotors are connected together both electrically and mechanically, and behave as an induction machine with P_p+P_c pole pairs.

Furthermore, if both stator windings are excited, but the rotor speed is not appropriate to create indirect cross coupling between their fields and put the machine in its desirable mode of operation (synchronous mode), BDFM will operate as two separate cascade machines. This condition happens when the speed controller fails to stabilize the machine in synchronous speed. If the rotational speed of the rotor space harmonic component in response to one of the stator winding field (e.g. power winding) with the same pole pairs as the other winding (e.g. control winding), does not match the field rotating speed of that winding (control winding), the winding (control winding) is short circuited from the harmonic component point of view, and vice versa.

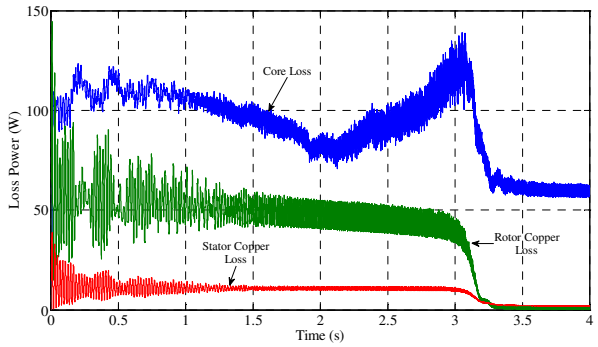

Figure 5. Core, rotor and stator copper losses in the simple induction mode.

Supposing that the power winding is supplied and the control winding is short circuited, the $B_{rp,P_c}(t,\theta_r)$ term in the rotor field, in response to the power winding field, induces an emf in the control winding. The induced voltage can be calculated by Equation(23). The control winding induced voltage can therefore be written as,

$$V_{c_a}^{rp,P_c}(t)=V_{c,\max}^{rp,P_c}(\omega_r)\sin\left(\left(\omega_p-P_r\omega_r\right)t-\varphi_c(\omega_r)\right) \quad (26)$$

$$V_{c_b}^{rp,P_c}(t)=V_{c,\max}^{rp,P_c}(\omega_r)\sin\left(\left(\omega_p-P_r\omega_r\right)t-\varphi_c(\omega_r)+\frac{2\pi}{3}\right) \quad (27)$$

$$V_{c_c}^{rp,P_c}(t)=V_{c,\max}^{rp,P_c}(\omega_r)\sin\left(\left(\omega_p-P_r\omega_r\right)t-\varphi_c(\omega_r)-\frac{2\pi}{3}\right) \quad (28)$$

The voltages generate current in shorted windings, and thus a rotating magnetic field in the air gap. The rotating field distribution, in the control winding and the rotor reference frames are presented in Equations(29) and (30), respectively

$$B_c^{rp,P_c}(t,\theta_c)=B_{c,\max}^{rp,P_c}(\omega_r)\cos\left(\left(\omega_p-P_r\omega_r\right)t+P_c\theta_c-\varphi_c(\omega_r)\right) \quad (29)$$

$$B_c^{rp,P_c}(t,\theta_r)=B_{c,\max}^{rp,P_c}(\omega_r)\cos\left(\left(\omega_p-P_p\omega_r\right)t+P_c\theta_r-\varphi_c(\omega_r)\right) \quad (30)$$

The phase and amplitude of the magnetic field are functions of the rotor speed. The amplitude is zero at ω_p/P_r and ω_p/P_p in the control winding and the rotor reference frames, respectively. For $\omega<\omega_n$ the magnetic field isclockwise (negative sequence), and for $\omega>\omega_n$ rotates anti-clockwise (positive sequence). Initially, the machine is supposed to operate below the natural speed.

The rotor bar induced voltage due to the magnetic field of Equation(30) is in the form of,

$$e_{rc}^{rp,P_c}(t,\theta_r)=lr\frac{\omega_p-P_p\omega_r}{P_c}B_{c,\max}^{rp,P_c}(\omega_r)\times\cos\left(\left(\omega_p-P_p\omega_r\right)t+P_c\theta_r-\varphi_c(\omega_r)\right) \quad (31)$$

The induced voltage in each loop can be calculated by subtracting its two bar voltages, as follows,

$$\Delta V_{rc}^{k,rp,P_c}(t,\theta_k)=\frac{2lrB_{c,\max}^{rp,P_c}(\omega_r)\left(\omega_p-P_p\omega_r\right)}{P_c}\times\sin\left(\pi P_c\left(\frac{1}{P_r}-\frac{1}{N_{rb}}\right)\right)\sin\left(\left(\omega_p-P_p\omega_r\right)t+P_c\theta_k-\varphi_c(\omega_r)\right) \quad (32)$$

The corresponding current in the k^{th} loop is presented inEquation (33).

$$i_{rc}^{k,rp,P_c}(t,\theta_k)=\frac{2lrB_{c,\max}^{rp,P_c}(\omega_r)\left(\omega_p-P_p\omega_r\right)}{P_c\sqrt{R_l^2+\left(\omega_p-P_p\omega_r\right)^2L_l^2}}\sin\left(\pi P_c\left(\frac{1}{P_r}-\frac{1}{N_{rb}}\right)\right)\times\sin\left(\left(\omega_p-P_p\omega_r\right)t+P_c\theta_k-\varphi_c(\omega_r)-\varphi_{nest}(\omega_r)\right) \quad (33)$$

The Fourier series of the MMF arises from the rotor nest current can be derived as follows,

$$\Im_{rc}^{rp,P_c}(t,\theta_k)=\sum_{n=1}^{\infty}\sum_{k=0}^{P_r-1}\frac{4lrB_{c,\max}^{rp,P_c}(\omega_r)\left(\omega_p-P_p\omega_r\right)}{n\pi P_c\sqrt{R_l^2+\left(\omega_p-P_p\omega_r\right)^2L_l^2}}\times\sin\left(\pi P_c\left(\frac{1}{P_r}-\frac{1}{N_{rb}}\right)\right)\sin\left(\pi n\left(\frac{1}{P_r}-\frac{1}{N_{rb}}\right)\right)\times$$
$$\sin\left(\left(\omega_p-P_p\omega_r\right)t+P_c\theta_k-\varphi_c(\omega_r)-\varphi_{nest}(\omega_r)\right)\cos\left(n\left(\theta_r-\theta_k\right)\right) \quad (34)$$

Production of the two terms containing θ_k in Equation(34) can be expanded as,

$$\frac{1}{2}\left[\sin\left(\left(\omega_p-P_p\omega_r\right)t+\left(P_c-n\right)\theta_k+n\theta_r-\varphi_c(\omega_r)-\varphi_{nest}(\omega_r)\right)+\sin\left(\left(\omega_p-P_p\omega_r\right)t+\left(P_c+n\right)\theta_k-n\theta_r-\varphi_c(\omega_r)-\varphi_{nest}(\omega_r)\right)\right] \quad (35)$$

Similar to the previous section, according to Equation(35), the rotor can produce $n=P_c+hP_r$ (clockwise) and $n=P_p+hP_r$ (anti-clockwise) space harmonic components in its air gap magnetic field. It should be noted that the directions in the parenthesis are for speeds below natural speed. Otherwise, the rotation direction of the control winding magnetic field and these terms would be reversed.

For $\omega<\omega_n$, the P_p pole pair harmonic of the rotor flux due to control winding field couples with the power winding field. Since they have identical direction and speed, it produces acceleration torque. However, for $\omega>\omega_n$, the field rotates in the opposite direction of the power winding field, which produces braking torque. As mentioned before, for $\omega<\omega_n$ and $\omega>\omega_n$the P_c pole pair harmonic fluxes of the rotor and control winding rotate in opposite and same direction with respect to the P_P pole pair harmonic fluxes, respectively, from the stationary point of view. This is the reason why BDFM operates near natural speed in this mode, and it operates similar to an induction machine with P_p+P_c pole pairs.

The torque can be calculated similar to the previous section asEquation (36),

$$\vec{T}=P_rrlI_{rc,\max}^{rp,P_c}(\omega_r)B_{p,\max}\sin\left(\pi P_c\left(\frac{1}{P_r}-\frac{1}{N_{rb}}\right)\right)\times\sin\left(\pi P_p\left(\frac{1}{P_r}-\frac{1}{N_{rb}}\right)\right)\cos\left(\varphi_c(\omega_r)+\varphi_{nest}(\omega_r)\right) \quad (36)$$

As expected, the torque for $\omega_r<\omega_p/P_r$ is positive, for $\omega_r<\omega_p/P_r$ is negative, and for $\omega_r=\omega_p/P_r$ is zero. Furthermore, the torque will be zero if $\omega_r=\omega_p/P_p$, because of zero emf induced in the rotor.

As stated, when both power and control windings are fed while rotor does not rotate at synchronous speed, there are two cascade machines with synchronous speeds of ω_p/P_r and ω_c/P_r.

Hence, the machine operating point would be between ω_c/P_r and ω_p/P_r and, one of the machines will act such as an applied load to the other.

Figures 6 and 7 illustrate the torque and rotor speed, respectively, when the control winding is short-circuited. As observed, the rotor rotates near natural speed.

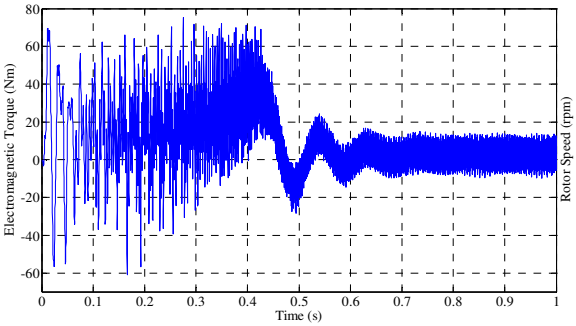

Figure 6. Electromagnetic torque in cascade mode of operation.

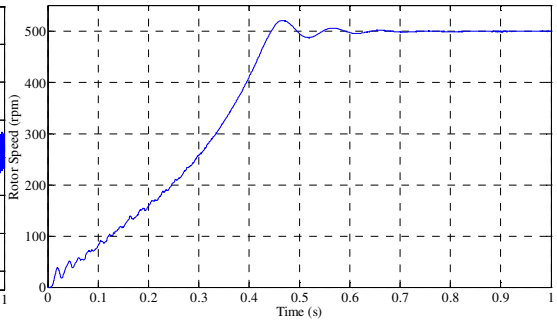

Figure 7. Rotor speed in cascade mode of operation.

The magnetic flux distribution is shown in Figure 8. It can be seen that the machine has 6 poles. Furthermore, it is obvious that the air gap magnetic field contains 2 and 4 pole pair space harmonics, while other harmonics have noticeable amplitude, because the relatively high speed of the power winding with respect to the rotor leads to high flux produced by the rotor.

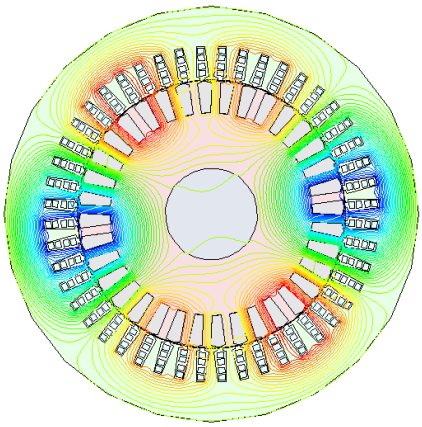

(a)

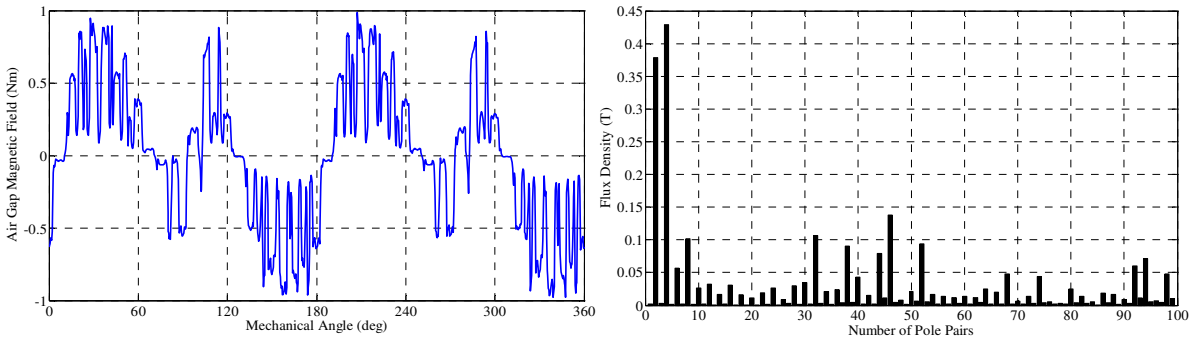

(b)(c)

Figure 8. Steady state operation in cascade induction mode (a) flux lines distribution (b) magnetic field vs. θr (c) space harmonic components of air gap field.

It is interesting to see the control winding current waveform while it is short circuited as shown in Figure 9. The control winding current amplitude and frequency are decreased when the speed increases to the natural speed, as expected.

Figure 10 shows the rotor current. The rotor current frequency (ω_p-$P_p\omega_r$) has been decreased with increasing rotor speed. The rotor frequency in this condition is (ω_p-$P_p\omega_r$)/2π=33.33, which is depicted in Figure 11.

The machine losses are divided into core as well as rotor and stator copper losses, which are shown in Figure 12. In this mode, the control winding is shorted, and therefore the currents are higher than simple induction mode. However, due to zero load torque, the steady state current and its corresponding losses are small.

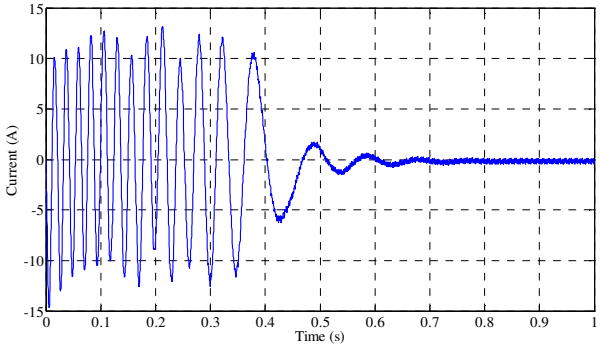

Figure 9. Control winding induced current in cascade mode.

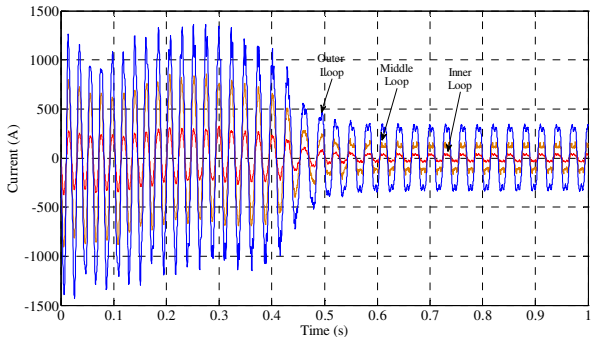

Figure 10. Rotor nest current.

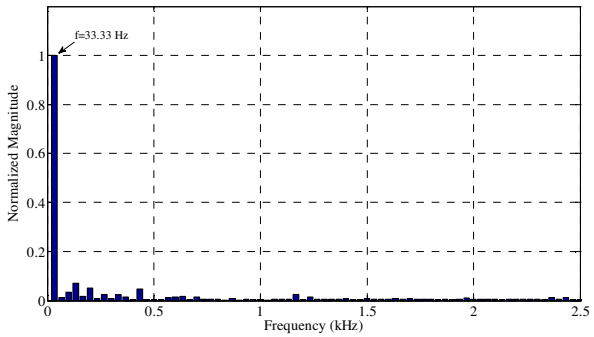

Figure11. Outer loop current FFT of a nest.

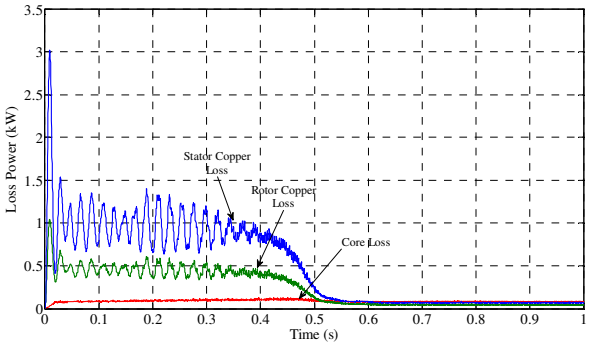

Figure 12. Core, rotor solid, and stator stranded losses.

The rotation speed is related to the load torque as in the case of conventional induction machine. Figures 13 and 14 show the electromagnetic torque and rotor speed in -10 and +20 Nm load torques, respectively.

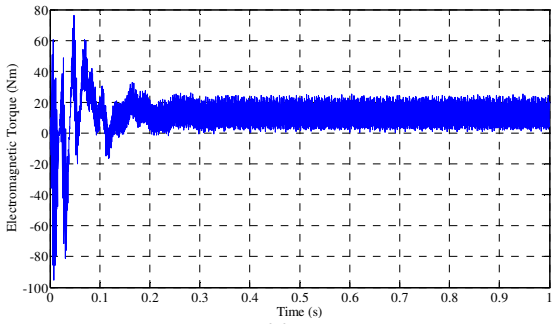

(a)

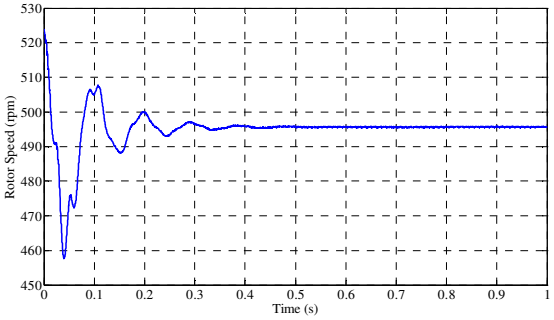

(b)

Figure 13. (a) Electromagnetic torque (b) speed in the cascade mode with -10 Nm load.

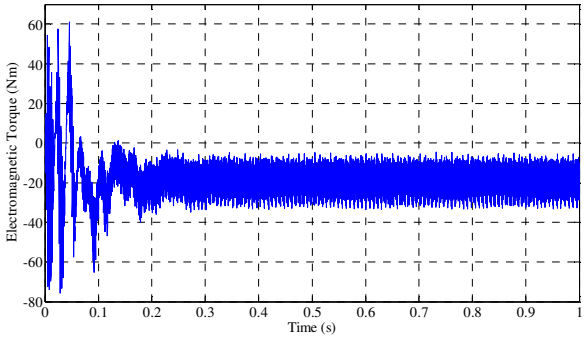

(a)

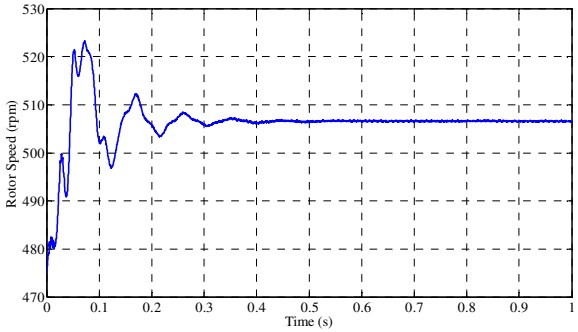

(b)

Figure 14. (a) Electromagnetic torque (b) speed in the cascade mode with +20 Nm load.

The torque-speed characteristic in cascade mode of operation (ω_n=500 rpm) is depicted in Figure 15 using Equation (36). The two operating points of Figures 13 and 14 which are indicated on this figure confirm the accuracy of the analytical procedure. Furthermore, the machine behavior is like an induction machine at the speeds close to the natural speed, and motoring and generating regions are clearly observable. The maximum torque in this mode is more than 50 times greater than the simple induction mode, which is the result of the high currents that was described before.

To show that the BDFM operates in asynchronous mode when both stator windings are excited, in the next simulation, the power winding is fed by a 100 V_{rms}, 50 Hz and the control winding by a 220 V_{rms}, 30 Hz voltage sources. As mentioned before, when the machine does not operate in synchronous mode, it works as two cascade machines, and the machine becomes stable between the natural speeds of two aforementioned machines. The rotor speed in this condition is shown in Figure 16.

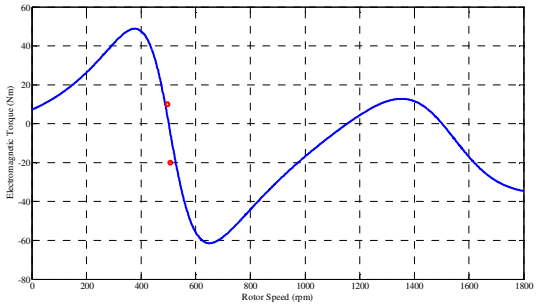

Figure 15. Torque-speed in cascade mode operation.

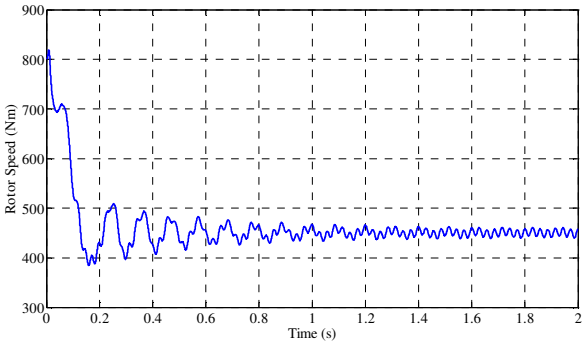

Figure 16. Rotor speed.

4. Conclusion

Brushless doubly-fed machine has an interesting but slightly complex structure and performance with desirable characteristic in variable speed applications such as wind turbines. A comprehensive and complete analytical study of the three modes of operation of BDFM is presented based on simple electromagnetic relations. The mechanism of direct and indirect cross couplings for each mode is explained in details and simulated by means of a 2D magnetodynamic finite element model.

The components of machine losses are obtained by FEM for each mode and their behavior with speed variation are explained. Also, the variations of losses portions are compared in three modes of operation. The torque-speed characteristics of asynchronous modes are depicted and the behavior compared with each other. Furthermore, the spatial harmonics in the air gap in three modes are illustrated and described. The performance of BDFM in synchronous mode relies on the pole number changing action by its nested loop rotor while the control winding field can affect the active and reactive powers of the PW. But the intermediate action of the rotor to change the pole pairs produces many unwanted space harmonics causing undesirable results in the machine behavior, for instance, increase iron loss, torque ripples, magnetizing currents, etc. Therefore, optimizing the structure of the machine is necessary to make it commercially applicable and bring it into industrial use.

5. References

[1] F. Lydall, "Improvement in polyphase induction motors," British *Patent 16839*, July 1902.

[2] L. J. Hunt, "A new type of induction machines," *J. IEE*, 1907, 39, pp. 648–677.

[3] F. Creedy, "Some development in multi-speed cascade induction motors," *J. IEE*, 1921, 59, pp. 511–532.

[4] A. R. Munoz and T. A. Lipo, "Dual stator winding induction machine drive," *IEEE Trans. Ind. Appl.*, 36, (5), pp. 1369–1379, 2000.

[5] Z. Wu and O. Ojo, "Coupled-Circuit Model Simulation and Airgap-field Calculation of a Dual Stator Winding Induction Machine," *IEE Proc.-Electr. Power Appl.*, pp. 387 – 400, Vol. 153, No. 3, May 2006.

[6] A. K. Wallace, R.Sp´ee, and H.K.Lauw, "The potential of brushless doublyfed machines for adjustable speed drives," in *Conference Record ofPulps and Paper Industry Technical Conference. Seattle: IEEE Industry Application Society,* pp. 45–50, June 20-22 1990.

[7] C. S. Brune, R. Sp´ee and A. K. Wallace, "Experimental evaluation of a variable-speed, doubly-fed wind-power generation system," *IEEE Trans. Industry Applications*, vol. 30, no. 3, pp. 648–655, May/June 1994.

[8] P. C. Roberts, "A study of Brushless Doubly-Fed (Induction) Machines" Ph. D. Thesis, University of Cambridge, Cambridge, England, Sep. 2004.

[9] P. J. Tavner, R. A. McMahon, P. C. Roberts, E. Abdi-Jalebi, X. Wang, M. Jagiela and T. Chick "Rotor & Design Performance for a BDFM". *In Proc. 17th Int. Conf. Electrical Machines (ICEM)*, Chania, Crete, Greece paper no. 439, Sep. 2006.

[10] A. R. W. Broadway and L. Burbridge, "Self-cascade machine: A low speed motor or high frequency brushless alternator", *Proc. Inst. Elect.Eng.*, vol. 117, no. 7, pp. 1529–1535, 1974.

[11] F. Bl´azquez, C. Veganzones, D. Ram´ırez and C. Platero, "Characterization of the Rotor Magnetic Field in a Brushless Doubly-Fed Induction Machine", *IEEE Trans. Energy Convers*., vol. 24, no. 3, Sep. 2009.

[12] H. Gorginpour, B. Jandaghi and H. Oraee, "Finite Element Analysis of Brushless Doubly Fed Machine Under Stator Winding Faults", *2nd Power Electronics, Drive Systems and Technologies Conference (PEDSTC)*, pp. 169 – 174, 2011.